

CERN-TH/96-225
DTP/96/78
LBNL-39238

Hadronic Antenna Patterns to Distinguish Production Mechanisms for Large- E_T Jets

John Ellis*

Theoretical Physics Division, CERN
1211 Geneva 23, Switzerland

Valery A. Khoze and W. James Stirling

Department of Physics, University of Durham,
Durham DH1 3LE, United Kingdom

ABSTRACT

Hadronic antenna patterns provide a tool able to diagnose different patterns of colour flow in large- E_T jet events. They reflect the underlying short-distance dynamics, and are sensitive to colour coherence and interference between the initial- and final-state partons. We discuss how hadronic antenna patterns may be used on large- E_T events from the Fermilab Tevatron or the CERN LHC to distinguish between conventional QCD and new physics production mechanisms such as a possible Z' boson or compositeness.

* This work was supported in part by the Director, Office of Energy Research, Office of Basic Energy Science of the U.S. Department of Energy, under Contract DE-AC03-76SF00098.

CERN-TH/96-225
DTP/96/78
LBNL-39238
August 1996

1 Introduction

Stimulated by recent data [1, 2] from the Fermilab Tevatron collider and by the prospects for future experiments with the CERN LHC, there is currently much interest in the possible interpretations of hadronic jets at large transverse energy E_T [3, 4]. It is premature to focus on speculative interpretations of the CDF data [1] until they have been reconciled satisfactorily with those from DØ [2], and until there is consensus whether it is possible to make a new global fit to parton distributions within the proton which accommodates the new data: for contrasting approaches, see [5, 6]. Nevertheless, it is appropriate to ask whether there are other ways in which one could in principle distinguish between a conventional QCD interpretation of large- E_T jet data and possible new physics such as a Z' boson [3] or compositeness [7]. This question is also important for future experiments at the LHC, which may well be confronted by it in their own large- E_T data a decade or so hence.

The purpose of this paper is to publicize a diagnostic tool which has been proposed in the literature but has not, to our knowledge, been discussed in connection with current large- E_T data: it is the pattern of hadronic energy flow around the large- E_T jet axes.

It has been known for a long time [8, 9] that the structure of multi-jet events in hard processes is influenced by the underlying colour dynamics at short distances. Detailed features of the parton shower, in particular the flow of colour quantum numbers, control the distributions of colour-singlet hadrons in the final state [10]. To leading order in the large- N_c limit, the analytic results for such antenna patterns coincide with the Lund string picture [11]. The first, and still the best, example of such a colour-related phenomenon is the so-called string [12] or drag [13] effect in $e^+e^- \rightarrow \bar{q}qg$ events, which is very well established experimentally, see for example Refs. [14, 15]. Colour coherence effects have also been seen very clearly in multi-jet events in $\bar{p}p$ collisions [16].

Patterns of hadron production in the large- E_T event plane have been measured, and shown [16] to differ significantly from the predictions of Monte Carlo models that do not include colour coherence and interference effects. On the other hand, the measurements agree very well with the predictions of Monte Carlo models, such as HERWIG [17], JETSET [18], ARIADNE [19] and JETRAD [20], which incorporate QCD colour coherence with interfering gluons¹. In particular, initial/final-state colour interference effects have been seen very clearly in the data. Thus the hadronic structure of a multi-jet event draws its colour portrait, and can be regarded as a “partonometer” mapping the basic interaction process.

A natural idea which has been proposed [8, 21, 22, 23, 24, 25, 26], is to use this “partonometry” to help distinguish new physics signals from backgrounds due to conventional QCD. One example of particular interest to the LHC is the possible use of rapidity gaps to favour Higgs production events [8, 23], and the pattern of QCD radiation in $t\bar{t}$ production has been examined [27]. Our suggestion here is to use “partonometry” to dissect the colour structure of the large- E_T jet events observed by CDF [1] and DØ [2], as a way to distinguish between conventional QCD and possible new production mechanisms such as a Z' boson [3] or compositeness [1, 7].

¹There are interesting differences between Monte Carlo results and the exact analytical QCD expectations [21], but these do not concern us here.

For any given pattern of colour flow between the initial and final states, there is a characteristic [21, 24, 26] pattern of gluon emission and hence hadronic energy flow in the transverse event plane. This is universal for hadron energies in the range $\Lambda_{QCD} \ll E \ll \sum E_T$, in the approximation of a large number of colours N_c . This should be a good approximation for secondary jet emission in the $qq(q\bar{q})$, qg and gg scattering processes of most interest for the Tevatron and the LHC. In this paper, we collect and compile the relevant formulae for conventional QCD, Z' and composite-model contributions to the large- E_T cross section, and discuss how these may be used to distinguish between these possible production mechanisms.

2 An Example of the Diagnostic Power of Hadronic Antenna Patterns

We begin by considering a simple illustrative example, the subprocess $q\bar{q} \rightarrow q'\bar{q}'$, where q and q' denote different quark flavours, which makes a distinctive contribution to the hadronic energy flow in large- E_T jet production at the Tevatron collider. In QCD, this process is dominated by s -channel gluon exchange. Suppose that there is an additional non-standard contribution from the s -channel exchange of a new, heavy Z' vector boson, $q\bar{q} \rightarrow Z' \rightarrow q'\bar{q}'$. If we assume, for simplicity, that the Z' has a vector coupling of strength g' to the quarks, then the matrix element squared is

$$\overline{\sum} |\mathcal{M}|^2 = \frac{g_s^4 C_F}{N_c} \frac{u^2 + t^2}{s^2} + 2g'^4 \frac{u^2 + t^2}{(s - M_{Z'}^2)^2 + M_{Z'}^2 \Gamma_{Z'}^2}, \quad (1)$$

where $C_F = (N_c^2 - 1)/2N_c$, and $M_{Z'}$ and $\Gamma_{Z'}$ are the Z' mass and width respectively. If the final-state quarks are produced at wide angle with transverse energy E_T then all the kinematic invariants are of order E_T^2 . For $E_T (\sim \sqrt{s}/2) \ll M_{Z'}$, the QCD process dominates. As E_T increases, the Z' contribution becomes more important, becoming maximal when $E_T \sim M_{Z'}/2$.

Next consider the emission of a soft gluon in the above process, i.e. $q(p_1) + \bar{q}(p_2) \rightarrow q'(p_3) + \bar{q}'(p_4) + g(k)$. In the soft gluon and large- N_c approximations, the matrix element is

$$\begin{aligned} \overline{\sum} |\mathcal{M}|^2 &= \frac{g_s^6 C_F}{N_c} \left(\frac{u^2 + t^2}{s^2} \right) \left\{ 2C_F([13] + [24]) \right\} \\ &+ 2g_s^2 g'^4 \left(\frac{u^2 + t^2}{(s - M_{Z'}^2)^2 + M_{Z'}^2 \Gamma_{Z'}^2} \right) \left\{ 2C_F([12] + [34]) \right\}. \end{aligned} \quad (2)$$

The distribution of soft gluon radiation is controlled by the basic antenna pattern (see for example Ref. [10])

$$[ij] \equiv \frac{p_i \cdot p_j}{p_i \cdot k \, p_j \cdot k} = \frac{1 - \mathbf{n}_i \cdot \mathbf{n}_j}{(1 - \mathbf{n} \cdot \mathbf{n}_i)(1 - \mathbf{n} \cdot \mathbf{n}_j)} \quad (3)$$

which describes the emission of soft primary gluons with energies E : $\Lambda_{QCD} \ll E \ll E_i, E_j$. The production of soft hadrons is then described by extra multiplicative cascading factors $N'_q(E_T)$ and $N'_g(E_T)$ within quark and gluon jets respectively (for details see Refs. [9, 13]):

$$N'_{q,g}(E_T) = \frac{dN_{q,g}}{d \ln E_T}, \quad (4)$$

where $N_{q,g}(E)$ is the particle multiplicity in an individual q, g jet with energy E . Asymptotically

$$N'_q(E_T) = \frac{C_F}{N_c} N'_g(E_T) \quad (5)$$

with

$$\frac{N'_g(E_T)}{N_g(E_T)} = \sqrt{\frac{4N_c\alpha_s(E_T)}{2\pi}} \left[1 + O\left(\sqrt{\frac{\alpha_s}{\pi}}\right) \right]. \quad (6)$$

Note that in the various asymmetry parameters (e.g. those used to describe the string effect) the cascading factors normally cancel. In the present study we will mainly be interested in the distribution of soft *jets* accompanying large- E_T jet production. We shall assume that this is well approximated by the distribution of a soft primary gluon which is given by matrix elements such as (2).

Returning to the $q\bar{q} \rightarrow q'\bar{q}'$ process, we see from (2) that the radiation pattern is different for the QCD and Z' contributions. At small E_T , the distribution is given by the sum of the [13] and [24] antennas. Soft gluon radiation is enhanced in the phase space region between the directions of partons 1 and 3 (and also between 2 and 4). If, however, at large E_T the Z' contribution is dominant, then the distribution is given by the sum of the [12] and [34] antennas, which yields a more symmetric radiation pattern. Thus the soft gluon distribution acts as a “partonometer” for probing the hard scattering process. In general, each type of $2 \rightarrow 2$ scattering will have its own distinctive radiation pattern.

In order to make the study more quantitative we must define appropriate kinematic distributions and then compute the contributions of the various subprocesses. In order to fully understand the differences between these, we first consider the soft gluon distribution at the parton-parton scattering level with fixed kinematics. The generic process is

$$a(p_1) + b(p_2) \rightarrow c(p_3) + d(p_4) + g(k), \quad (7)$$

where the gluon is soft relative to the two large- E_T partons c and d . Ignoring the gluon momentum in the energy-momentum constraints, and using the notation $p^\mu = (E, p_x, p_y, p_z)$, we write

$$\begin{aligned} p_1^\mu &= (E_T \cosh \eta, 0, 0, E_T \cosh \eta), \\ p_2^\mu &= (E_T \cosh \eta, 0, 0, -E_T \cosh \eta), \\ p_3^\mu &= (E_T \cosh \eta, 0, E_T, E_T \sinh \eta), \\ p_4^\mu &= (E_T \cosh \eta, 0, -E_T, -E_T \sinh \eta), \\ k^\mu &= (k_T \cosh(\eta + \Delta\eta), k_T \sin \Delta\phi, k_T \cos \Delta\phi, k_T \sinh(\eta + \Delta\eta)). \end{aligned} \quad (8)$$

This is the appropriate form for studying the angular distribution of the soft gluon jet relative to the large- E_T jet 3, the separation between these being parametrized by $\Delta\eta$ and $\Delta\phi$. Alternative variables, more suited to the experimental analysis, are the radial and polar angle variables in the “LEGO plot”:

$$\begin{aligned} \Delta\eta &= \Delta R \cos \beta, \\ \Delta\phi &= \Delta R \sin \beta. \end{aligned} \quad (9)$$

which are defined in such a way that the LEGO-plot separation between soft jet k and hard jet p_3 is constant: $R(k, p_3) = \sqrt{\Delta\eta^2 + \Delta\phi^2} = \Delta R$, ($0 \leq \Delta R < \infty$), and the azimuthal orientation of jet k around jet p_3 in the LEGO plot is parametrized by the angle β , ($0 \leq \beta < 2\pi$).

In terms of these variables, the soft gluon phase space is

$$\frac{1}{(2\pi)^3} \frac{d^3k}{2E_k} = \frac{1}{16\pi^3} k_T dk_T \Delta R d\Delta R d\beta. \quad (10)$$

We will be particularly interested in the behaviour of the cross section as a function of β for fixed $k_T, \Delta R$ and fixed E_T, η .

Note that the β distributions presented here should be considered only as instructive examples. In the quantitative study of interference phenomena it may prove useful to exploit other variables, for example the α variable used in the CDF analysis [16]. Another useful discriminator for studying the underlying scattering dynamics is provided by correlations of the type [9, 29]

$$\frac{N_{UR} \pm N_{LL} - N_{UL} \mp N_{LR}}{N_{UR} + N_{LL} + N_{UL} + N_{LR}}, \quad (11)$$

where N_{ij} is the number of events with the soft jet in the angular region ij of the scattering plane (i denotes the upper (U) or lower (L) quadrant and j denotes the left (L) or right (R) quadrant).

There are a large number of processes of type (7). The matrix elements are collected in the Appendix. In addition to the QCD contributions, we include also the contributions from Z' exchange to $qq \rightarrow qq$ scattering (including processes related by crossing), assuming an interaction of the form

$$g' \bar{\psi}_q \gamma_\mu (v_q + a_q \gamma_5) \psi_q Z'^\mu. \quad (12)$$

For illustrative purposes in our numerical calculations, we use the set of parameters suggested in Ref. [28] on the basis of a combined fit to LEP and CDF data:

$$v_u = 1.2, \quad a_u = 3.2, \quad v_d = -1, \quad a_d = 1, \quad (13)$$

with $g' = e/\sin\theta_W$ and $M_{Z'} = 1$ TeV.

We first show results for a very simple kinematic configuration, $2 \rightarrow 2$ scattering at 90° in the parton centre-of-mass frame, i.e. $\eta = 0$ in Eq. (8). We fix k_T and E_T at 10 GeV and 100 GeV respectively, so that $k_T \ll E_T$, and study the angular (β) distribution of the soft gluon jet around one of the two large- E_T jets (p_3), see Fig. 1. Following the $D\emptyset$ analysis [2], we use the variables ΔR and β defined above. For small ΔR , the radiation pattern is dominated by the matrix-element singularity when k and p_3 are parallel: the β distribution is constant and simply reflects the colour charge of the emitting parton. For large ΔR , the pattern is sensitive to the colour flow in the scattering process. We display results for $\Delta R = 1$, which is typical of the values used in the experimental analyses. Figure 2 shows the soft gluon distribution for various $2 \rightarrow 2$ scattering processes as a function of β^2 . The quantity plotted is the ratio of the $2 \rightarrow 3$ and $2 \rightarrow 2$ matrix elements, omitting an overall factor of g_s^2 . The

²For the choice of kinematics adopted here, the distribution is symmetric in $\beta \leftrightarrow 2\pi - \beta$.

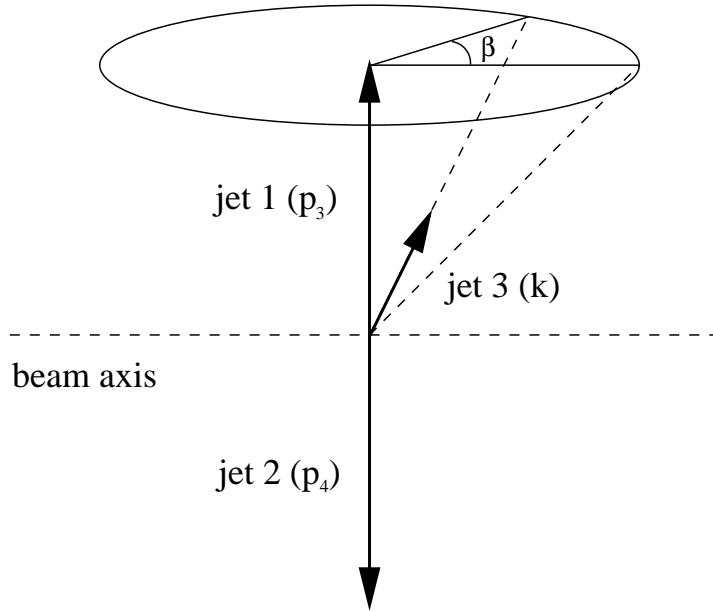


Figure 1: Jet configuration for the numerical studies described in the text.

characteristics of these distributions can be understood in terms of the colour strings linking the initial- and final-state partons, see for example Ref. [10]. Notice in particular that the distribution for the $gg \rightarrow gg$ process is approximately constant, reflecting the comparable contributions to the radiation pattern from the incoming and outgoing gluons. For the $qg \rightarrow gq$ and $qg \rightarrow qq$ processes, the distributions are peaked in the backward ($\cos \beta < 0$) direction. For the former, this corresponds to the colour string between an outgoing 8 and $\bar{8}$, as for $gg \rightarrow gg$.

Also shown in Fig. 2 is the radiation pattern for the process $q\bar{q} \rightarrow Z' \rightarrow q'\bar{q}'$. In this case the distribution has the simple analytic form

$$\frac{d\mathcal{W}}{d\beta} = 2C_F([12] + [34]) = \frac{4C_F}{k_T^2} \left[1 + \frac{1}{\cosh^2(\Delta R \cos \beta) - \cos^2(\Delta R \sin \beta)} \right]. \quad (14)$$

Note that the [12] antenna corresponding to gluon radiation from the initial-state $q\bar{q}$ gives a contribution which is *independent* of β . In the large- N_c limit, the corresponding QCD process gives the distribution

$$\frac{d\mathcal{W}}{d\beta} \rightarrow 2C_F([13] + [24]) = \frac{4C_F}{k_T^2} \left[\frac{\cosh^2(\Delta R \cos \beta) + \sinh(\Delta R \cos \beta) \cos(\Delta R \sin \beta)}{\cosh^2(\Delta R \cos \beta) - \cos^2(\Delta R \sin \beta)} \right]. \quad (15)$$

In contrast to (14), this distribution is not symmetric about $\beta = 90^\circ$. For a heavy Z' with sizeable couplings to quarks, we would expect a transition from the “QCD” radiation pattern at low E_T to the “ Z' ” radiation pattern at high E_T . This is illustrated in Fig. 3, for the parton scattering process $u\bar{u} \rightarrow d\bar{d}$. The distribution is obtained from Eq. (A4) and

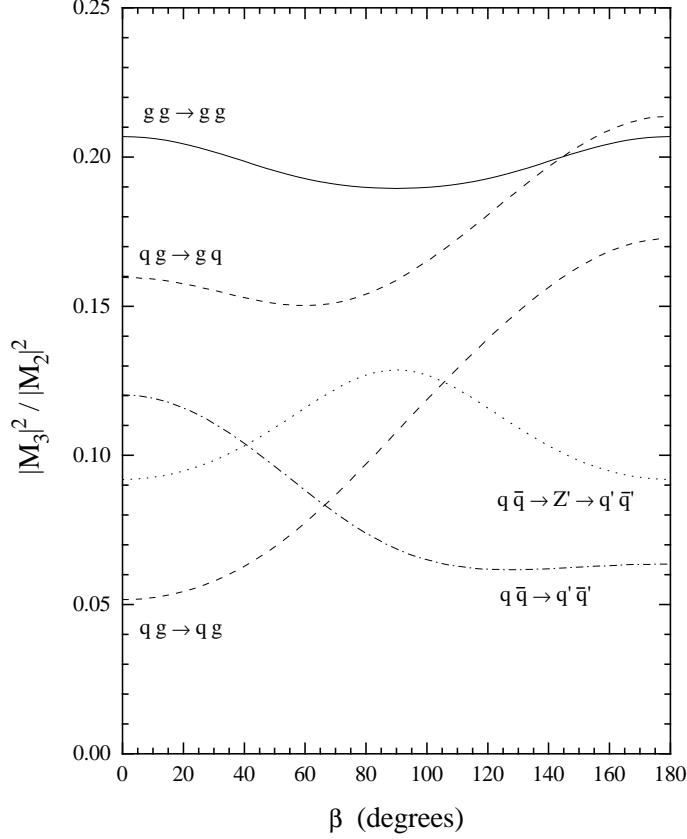


Figure 2: Ratio of the $2 \rightarrow 3$ and $2 \rightarrow 2$ matrix elements as a function of the soft gluon azimuthal angle about the large- E_T jet, for various QCD and Z' subprocesses.

contains the contributions from the QCD and Z' processes, and their interference. For these simple kinematics, $E_T = M_{Z'}/2 = 500$ GeV corresponds to the resonance peak where the Z' contribution is maximal. Notice the significant change in the shape of the distribution as E_T approaches this value from below.

The interference between the QCD and Z' contributions deserves further discussion. By colour conservation, this is absent in the leading-order (no gluon radiation) amplitudes, and at $O(\alpha_s)$ is suppressed by a single power of N_c in the large- N_c limit, see Eq. (A4). The corresponding antenna pattern is given by

$$\frac{d\mathcal{W}_{\text{int}}}{d\beta} \rightarrow 2C_F([13] + [24] - [14] - [23]) = \frac{8C_F}{k_T^2} \left[\frac{\sinh(\Delta R \cos \beta) \cos(\Delta R \sin \beta)}{\cosh^2(\Delta R \cos \beta) - \cos^2(\Delta R \sin \beta)} \right], \quad (16)$$

where we have substituted the kinematic variables relevant to Fig. 3, i.e. $\eta = 0$. The interference contribution vanishes on the Z' resonance (i.e. for $E_T = 500$ GeV in Fig. 3) and is everywhere numerically small relative to the sum of the QCD and Z' amplitudes squared.

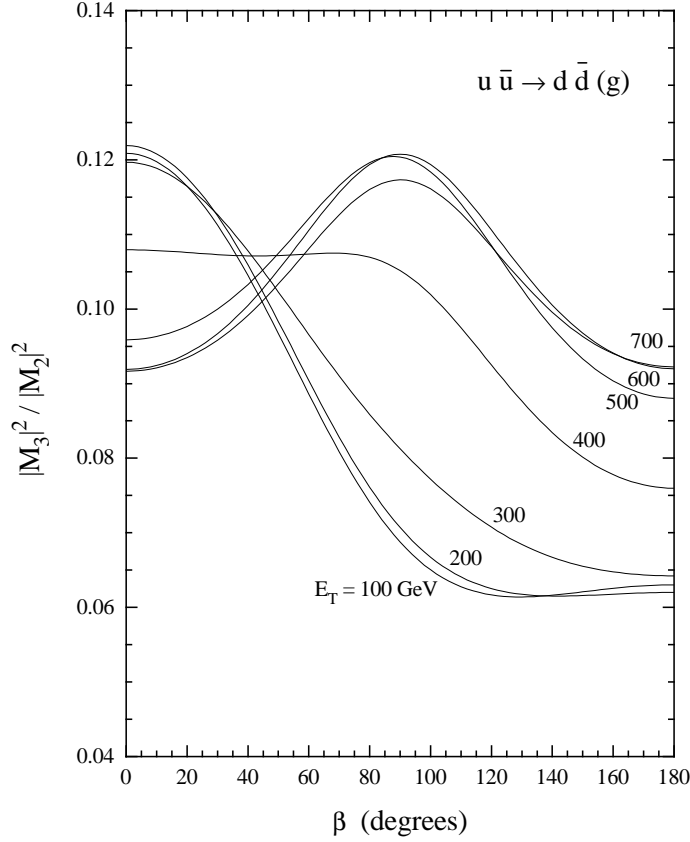


Figure 3: Ratio of the $2 \rightarrow 3$ and $2 \rightarrow 2$ matrix elements as a function of the soft gluon azimuthal angle about the large- E_T jet for the $u\bar{u} \rightarrow d\bar{d}(g)$ subprocess, including QCD and Z' contributions.

As an illustration, Fig. 4 shows the decomposition of the $u\bar{u} \rightarrow d\bar{d}(g)$ radiation pattern for $E_T = 400$ GeV. For this kinematic configuration (90° scattering in the parton centre-of-mass frame) the interference is antisymmetric about $\beta = 90^\circ$. Note that the antenna pattern in Eq. (16) is asymmetric with respect to the interchange $p_3 \leftrightarrow p_4$ and therefore vanishes if one does not distinguish the final-state jets. It also vanishes after integration over the angles between the $q\bar{q}$ and $q'\bar{q}'$ antennae, see Ref. [27]. This can readily be seen by writing Eq. (16) as

$$2C_F([13] + [24] - [14] - [23]) = -\frac{8C_F}{|\vec{k}|^2} \left[\frac{\cos \phi}{\sin \theta_1 \sin \theta_3} \right], \quad (17)$$

where $\theta_{1,3}$ is the polar angle between the \vec{k} and $\vec{p}_{1,3}$ vectors, and ϕ is the azimuthal angle between the planes formed by \vec{k}, \vec{p}_1 and \vec{k}, \vec{p}_3 .

More generally, the interference between diagrams with different colour flows at the amplitude level destroys the factorization of the radiation pattern into a product of the eikonal

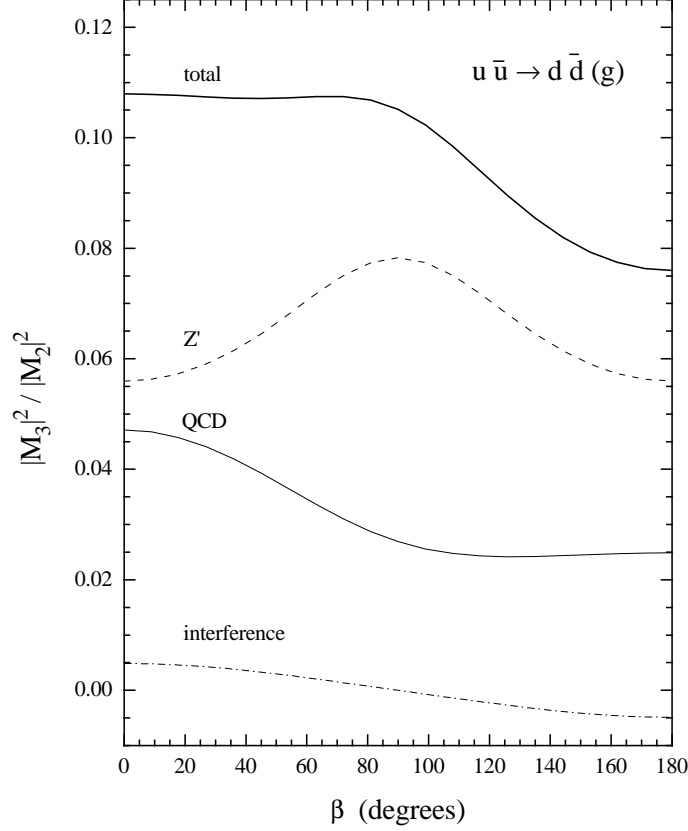


Figure 4: Decomposition of the $u\bar{u} \rightarrow d\bar{d}(g)$ radiation pattern of Fig. 3, for $E_T = 400$ GeV. The curves represent the various contributions to the $2 \rightarrow 3$ matrix element squared, normalized in each case to the total QCD+ Z' $2 \rightarrow 2$ matrix element squared.

antenna factors and the lowest-order cross sections. Note that an analogous interference contribution induces “colour interconnection effects” in the pattern of gluon radiation accompanying $e^+e^- \rightarrow q_1\bar{q}_2q_3\bar{q}_4$ events, see Ref. [30].

We conclude this section with some remarks on the validity of the soft gluon and large- N_c approximations. Consider, for example, the QCD $2 \rightarrow 3$ process $qq' \rightarrow qq'g$. The exact matrix element is [31]

$$\overline{\sum}|\mathcal{M}|^2(\text{exact}) = \frac{g_s^6 C_F}{N_c} \left(\frac{s^2 + s'^2 + u^2 + u'^2}{2tt'} \right) \left\{ 2C_F([14] + [23]) + \frac{1}{N_c}[12; 34] \right\}, \quad (18)$$

where

$$\begin{aligned} s &= (p_1 + p_2)^2, & t &= (p_1 - p_3)^2, & u &= (p_1 - p_4)^2, \\ s' &= (p_3 + p_4)^2, & t' &= (p_2 - p_4)^2, & u' &= (p_2 - p_3)^2. \end{aligned} \quad (19)$$

The soft gluon approximation which we have used in the above calculations corresponds to

$$\overline{\sum} |\mathcal{M}|^2(\text{soft}) = \frac{g_s^6 C_F}{N_c} \left(\frac{s^2 + u^2}{t^2} \right) \left\{ 2C_F([14] + [23]) + \frac{1}{N_c}[12; 34] \right\}, \quad (20)$$

with $s = s'$ etc. Making the large- N_c approximation, the above expression simplifies further to

$$\overline{\sum} |\mathcal{M}|^2(\text{soft, large-}N_c) = \frac{g_s^6 C_F}{N_c} \left(\frac{s^2 + u^2}{t^2} \right) \left\{ 2C_F([14] + [23]) \right\}. \quad (21)$$

To test the validity of these approximations, we consider the ratios of the matrix elements in (20) and (21) to that in (18). For the latter, we use exact $2 \rightarrow 3$ kinematics defined by

$$\begin{aligned} p_1^\mu &= (E, 0, 0, E), \\ p_2^\mu &= (E, 0, 0, -E), \\ p_3^\mu &= (E_T \cosh \eta, 0, E_T, E_T \sinh \eta), \\ p_4^\mu &= (E_4, -k_T \sin \Delta\phi, -E_T - k_T \cos \Delta\phi, -E_T \sinh \eta - k_T \sinh(\eta + \Delta\eta)), \\ k^\mu &= (k_T \cosh(\eta + \Delta\eta), k_T \sin \Delta\phi, k_T \cos \Delta\phi, k_T \sinh(\eta + \Delta\eta)). \end{aligned} \quad (22)$$

with $E_4 = |\mathbf{p}_4|$ and $2E = E_3 + E_4 + E_k$. Figure 5 shows the ratio of the approximate and exact matrix elements as a function of β for $\eta = 0$, $\Delta R = 1$, and $k_T/E_T = 0.1, 0.2$. The solid lines indicate that the corrections to the radiation pattern in the soft approximation scale as $O(k_T/E_T)$. The difference between the dashed and solid lines is $O(10\%)$, consistent with $O(1/N_c^2)$ corrections to the large- N_c approximation. The curves in Fig. 5 attain their maximum deviation from unity at the end-points, $\cos \beta = \pm 1$, since for this choice of kinematics the ratio of the gluon energy to that of jet 3 is $E_k/E_3 = \cosh(\cos \beta) k_T/E_T$, which for fixed k_T/E_T is maximal at large $|\cos \beta|$. In what follows we shall use the soft gluon matrix elements listed in the Appendix, retaining the complete set of antennas valid for arbitrary N_c .

3 Convolution with Parton Distributions

To obtain realistic predictions for the distribution of soft gluon radiation accompanying large- E_T jets at, say, the Tevatron $\bar{p}p$ collider, we must convolute the matrix elements with appropriate parton distributions. This then gives a E_T -dependent mixture of the various distributions shown in Fig. 2. To avoid unnecessary complications from kinematics, and to make contact with the parton-level results obtained above, we consider the production of a pair of large- E_T jets at zero rapidity in the laboratory frame, i.e. $E_{T3} = E_{T4} = E_T$, $\eta_3 = \eta_4 = 0$. The leading-order inclusive two-jet cross section is

$$\begin{aligned} \frac{d^3\sigma}{d\eta_3 d\eta_4 dE_T} &= \frac{E_T}{8\pi x_1 x_2 s^2} \sum_{a,b,c,d=q,\bar{q},g} f_a(x_1, \mu^2) f_b(x_2, \mu^2) \\ &\times \frac{1}{1 + \delta_{cd}} \overline{\sum} |\mathcal{M}(ab \rightarrow cd)|^2, \end{aligned} \quad (23)$$

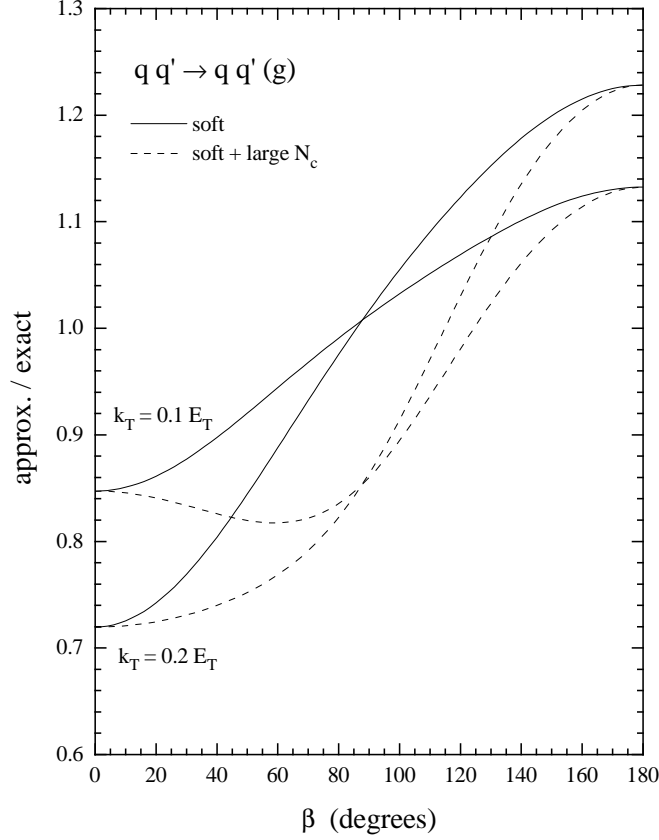


Figure 5: Ratio of approximate and exact matrix elements, as described in the text.

with $x_1 = x_2 = x_T \equiv 2E_T/\sqrt{s}$ for our choice of kinematics. The symmetry factor δ_{cd} is 1(0) for identical (non-identical) partons in the final state. Next-to-leading order corrections to the inclusive cross section are approximately taken into account by the scale choice $\mu = E_T/2$. We use the recent MRS(R2) parton set ($\alpha_s(M_Z^2) = 0.120$), which gives a good overall description of the CDF and DØ large- E_T inclusive jet cross section [32]. The corresponding two-jet + soft gluon inclusive cross section is

$$\begin{aligned} \frac{d^6\sigma}{dk_T d\Delta R d\beta d\eta_3 d\eta_4 dE_T} &= \frac{k_T \Delta R E_T}{128\pi^4 x_1 x_2 s^2} \sum_{a,b,c,d=q,\bar{q},g} f_a(x_1, \mu^2) f_b(x_2, \mu^2) \\ &\times \frac{1}{1 + \delta_{cd}} \overline{\sum} |\mathcal{M}(ab \rightarrow cd + g)|^2. \end{aligned} \quad (24)$$

For the additional factor of α_s coming from the soft gluon emission we use $\mu = k_T$. As before, we consider the ratio of the cross sections in (24) and (23) as a function of the soft

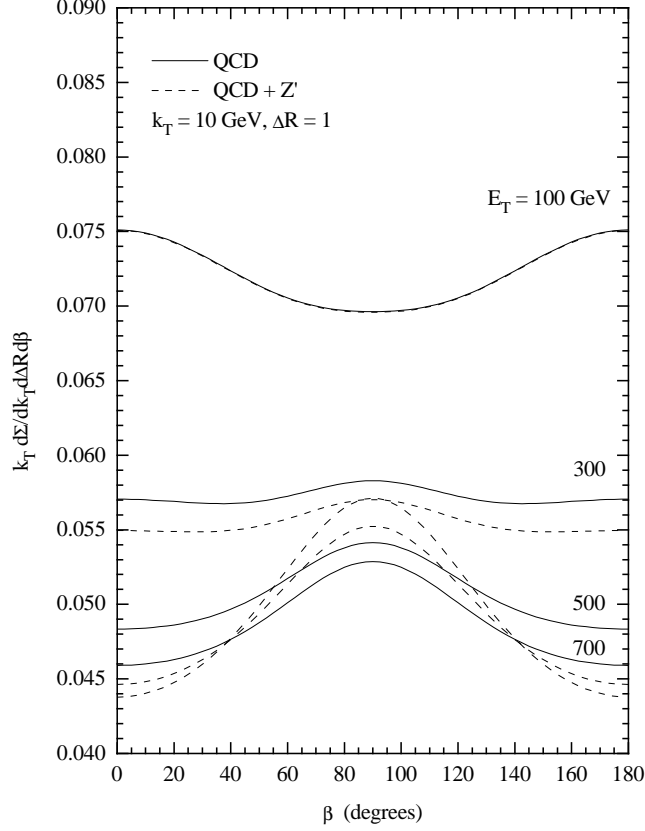


Figure 6: Radiation pattern for the soft gluon jet in large- E_T dijet production in $\bar{p}p$ collisions at 1.8 TeV. All scattering processes are included, weighted by the appropriate parton distributions.

gluon variables:

$$\frac{d\Sigma}{dk_T d\Delta R d\beta} \equiv \left[\frac{d^3\sigma}{d\eta_3 d\eta_4 dE_T} \right]^{-1} \frac{d^6\sigma}{dk_T d\Delta R d\beta d\eta_3 d\eta_4 dE_T} . \quad (25)$$

Figure 6 shows the distribution $k_T d\Sigma/dk_T d\Delta R d\beta$ as a function of β for $k_T = 10$ GeV, $\Delta R = 1$ and various values of E_T . The solid curves are the QCD predictions, and the dashed curves include also the Z' contribution with same parameters as in the previous figures. We note the following.

- (i) All the distributions are symmetric about $\beta = 90^\circ$. This is due to our choice of symmetric large- E_T jet kinematics, and because we have summed over all combinations of partons (jets) in the initial and final states, e.g. $qg, gq \rightarrow qg, gq$.³

³By varying the jet rapidities one can preferentially select, say, the qg initial state over the gq initial state and expose the asymmetries of the qg radiation pattern in Fig. 2.

- (ii) For the QCD curves, the radiation pattern decreases in magnitude as E_T increases. This is simply a colour charge effect: as one moves from small E_T to large E_T the dominate subprocess scattering changes from gg to qg to $q\bar{q}$.
- (iii) The effect of the Z' contribution is clearly visible in the dashed curves at large E_T . As already seen in Fig. 2, the Z' radiation pattern has a peak at $\beta = 90^\circ$. The effect is most significant for $E_T = M_{Z'}/2$, as expected. But note also a similar (though weaker) peak structure in the QCD ‘background’. This arises from the $q\bar{q} \rightarrow q\bar{q} + g$ process which, for the t -channel gluon exchange contribution, has a dominant $C_F([12] + [34])$ antenna pattern as for $q\bar{q} \rightarrow Z' \rightarrow q\bar{q}$. The effect only arises for the identical quark process – there is no such t -channel contribution for $q\bar{q} \rightarrow q'\bar{q}' + g$.
- (iv) This latter comment suggests a method for further enhancing the Z' signal, or other new physics contributions, over the QCD background. Figure 7 shows the effect of selecting only the $b\bar{b}$ component of the final state in Fig. 6. Such a selection could in principle be achieved experimentally by means of a vertex detector. At small E_T the dominant process is $gg \rightarrow b\bar{b}$ with a large, approximately flat β distribution. At large E_T , the QCD process $q\bar{q} \rightarrow b\bar{b}$ has a dominant antenna pattern given by $C_F([13] + [24])$, which is very different from the $C_F([12] + [34])$ pattern of $q\bar{q} \rightarrow Z' \rightarrow b\bar{b}$. We note in passing that purely in the context of QCD, a $b\bar{b}$ subsample of the large- E_T dijet events should exhibit a markedly different distribution of soft hadronic radiation.

4 Application to Composite Models

If the quarks and leptons of the Standard Model are composite objects, one would expect to see new four-fermion contact interactions well below the scale Λ characterizing the size of the composite states [7]. In particular, a four-quark contact interaction would produce a flattening of the large- E_T jet distribution at scales $E_T \sim \Lambda$. The colour structure of such a contact interaction would generate a distinctive antenna pattern of soft radiation, which could be used to distinguish between standard QCD and different types of contact interactions between quarks.

It is straightforward to write down the most general $SU(3) \times SU(2) \times U(1)$ invariant four-quark contact interaction, see for example Ref. [33]. The generic form is

$$\mathcal{L}_c = \frac{4\pi}{2\Lambda^2} \sum \bar{q}\gamma^\mu q \bar{q}\gamma_\mu q, \quad (26)$$

where the sum is over the colour, flavour and helicity labels carried by the quark fields. There are two possible colour structures for such interactions:

$$\bar{q}_i\gamma^\mu q_i \bar{q}_j\gamma_\mu q_j, \quad \bar{q}_i T_{ik}^a \gamma^\mu q_k \bar{q}_j T_{jl}^a \gamma_\mu q_l, \quad (27)$$

where $i, j, k, l = 1, 2, 3$ are colour labels and the T_{ij}^a ($a = 1, \dots, 8$) are the $SU(3)$ colour matrices of QCD. The two terms in Eq. (27) correspond to colour singlet and octet exchange respectively. Combining these new contact interactions with those of standard QCD, one

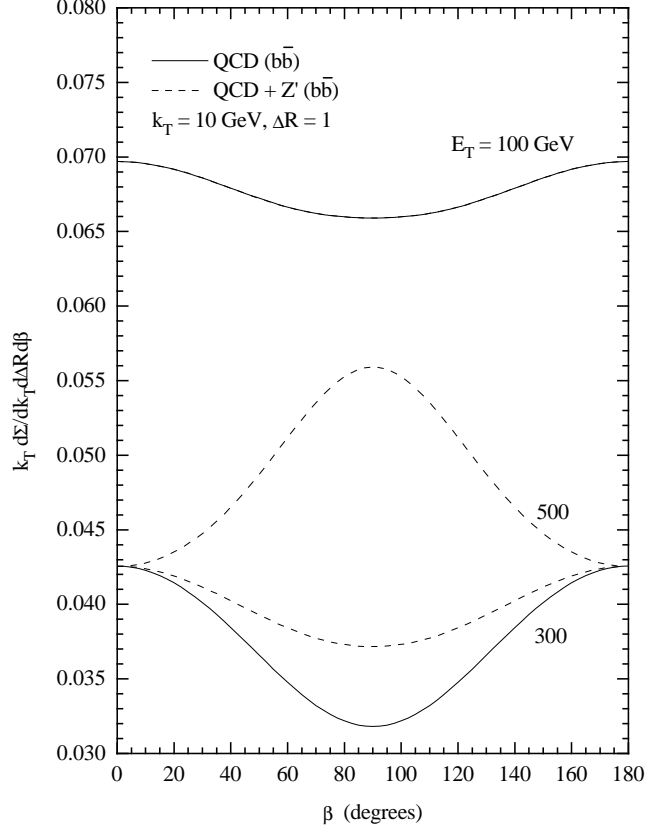


Figure 7: As for Fig. 6, except that only the large- E_T $b\bar{b}$ final state is included. The QCD (solid) curves for $E_T = 300$ GeV and 500 GeV are indistinguishable.

obtains additional contributions to the $2 \rightarrow 2$ scattering processes involving quarks. For example, for the $qq \rightarrow qq$ amplitude squared, the additional contributions are of order Λ^{-4} (contact interaction squared) and $(t\Lambda^2)^{-1}$, $(u\Lambda^2)^{-1}$ for the QCD-contact interference.

The additional contributions to the radiation pattern can be calculated in the same way. As a specific example, we consider the most widely used interaction of type (26), involving the product of left-handed, colour-singlet, isoscalar first-generation quark currents:

$$\mathcal{L}_c = \frac{4\pi\eta}{2\Lambda^2} \sum_{i,j=1,3} \bar{q}_{iL}\gamma^\mu q_{iL} \bar{q}_{jL}\gamma_\mu q_{jL} , \quad (28)$$

where $q = (u, d)$ and $\eta = \pm 1$ determines whether the interference with the standard QCD interaction is constructive or destructive. In fact the effect of such an interaction can be readily obtained as a limiting case of the Z' results listed in the Appendix, specifically by

setting $v' = -a' = 1$ and taking the limit

$$M_{Z'}, g' \rightarrow \infty \quad \text{with} \quad \left(\frac{2g'}{M_{Z'}} \right)^2 = -\frac{4\pi\eta}{\Lambda^2} \quad \text{fixed.} \quad (29)$$

Thus for $ud \rightarrow ud + g$ we obtain (cf. A5)

$$\begin{aligned} \overline{\sum} |\mathcal{M}|^2 &= \frac{g_s^6 C_F}{N_c} \left(\frac{s^2 + u^2}{t^2} \right) \left\{ 2C_F([14] + [23]) + \frac{1}{N_c} [12; 34] \right\} \\ &+ \frac{(4\pi)^2 g_s^2 s^2}{\Lambda^4} \left\{ 2C_F([13] + [24]) \right\} + \frac{4\pi\eta g_s^4 s^2}{t\Lambda^2} \frac{C_F}{N_c} \left\{ 2([14] + [23] - [12] - [34]) \right\}. \end{aligned} \quad (30)$$

Radiation patterns for the other quark interactions can be obtained in a similar way. The numerical results will be qualitatively similar to those for the heavy Z' presented in Sections 2 and 3.

For a four-quark interaction corresponding to *colour octet* exchange, the effect on the radiation pattern at large E_T will be much less dramatic, since the antenna structure for, say, $q\bar{q} \rightarrow q\bar{q}$ scattering will be the same for both standard gluon exchange and for the contact interaction. In principle, therefore, the radiation pattern provides a unique method for unravelling the colour structure of a new four-quark interaction.

5 Conclusions

We have demonstrated in this paper how the hadronic antenna pattern due to gluon radiation may be used as a diagnostic tool which reveals the short-distance colour flow dynamics, and hence may be used to discriminate between different production mechanisms for large- E_T jets in $\bar{p}p$ or pp collisions. In particular, we have discussed in some detail the hadronic antenna pattern associated with the production of a Z' boson decaying into jet pairs, and contrasted it with that predicted by conventional QCD. We have also related contact interactions with different colour exchanges to the QCD and Z' cases, so that they may also be distinguished by their hadronic antenna patterns.

The diagnostic tool provided by these hadronic antenna patterns may be useful in the analysis of current large- E_T jet events at the Fermilab $\bar{p}p$. If they turn out to have some component beyond conventional QCD, gluon radiation may help pin down the additional production mechanism. Even if the current large- E_T data turn out to be satisfactorily fitted within conventional QCD, this tool may be a useful addition to the kit of analysis methods to be applied to future hadronic-jet data at even larger E_T at the LHC.

Finally, we note that the technique of using hadronic antenna patterns as a probe of new physics has many other applications other than those discussed in detail in this study. For example, in Higgs production by gluon-gluon fusion at hadron colliders the density of hadrons in the plateau corresponding to the incoming partons (the [12] antenna) should be approximately twice as large as for Z' production. Another application is to final states in deep-inelastic scattering, where the technique could be used, for example, as a probe of “rapidity-gap” physics.

Acknowledgements

We thank G. Blazey, Yu. Dokshitzer, M. Mangano and N. Varelas for useful comments and discussions. The work of J.E. was supported in part by the Director, Office of Energy Research, Office of Basic Energy Science of the U.S. Department of Energy, under Contract DE-AC03-76SF00098. The work of VAK and WJS was supported in part by the UK PPARC and the EU Programme “Human Capital and Mobility”, Network “Physics at High Energy Colliders”, contract CHRX-CT93-0357 (DG 12 COMA).

Appendix

The following expressions are for the spin/colour summed/averaged matrix elements for the scattering processes

$$a(p_1) + b(p_2) \rightarrow c(p_3) + d(p_4) + g(k) \quad (\text{A1})$$

in the soft gluon approximation. The QCD matrix elements are taken from Refs. [8, 21, 26]. The antennae are defined by

$$\begin{aligned} [ij] &= \frac{p_i \cdot p_j}{p_i \cdot k \, p_j \cdot k} , \\ [ij; kl] &= 2[ij] + 2[kl] - [ik] - [il] - [jk] - [jl] . \end{aligned} \quad (\text{A2})$$

and

$$s = (p_1 + p_2)^2 , \quad t = (p_1 - p_3)^2 , \quad u = (p_1 - p_4)^2 . \quad (\text{A3})$$

The Z' couplings are defined in Eq. (12), with (v, a) and (v', a') denoting the vector, axial couplings of the Z' to quarks q and q' respectively. Only a subset of all the possible processes are listed; the rest can be obtained by crossing.

$$q(p_1) + \bar{q}(p_2) \rightarrow q'(p_3) + \bar{q}'(p_4) + g(k)$$

$$\begin{aligned} \overline{\sum} |\mathcal{M}|^2 &= \frac{g_s^6 C_F}{N_c} \left(\frac{u^2 + t^2}{s^2} \right) \left\{ 2C_F([13] + [24]) + \frac{1}{N_c} [14; 23] \right\} \\ &+ 2g_s^2 g'^4 \left(\frac{(u^2 + t^2)\{(v^2 + a^2)(v'^2 + a'^2)\} + (u^2 - t^2)\{4vav'a'\}}{(s - M_{Z'}^2)^2 + M_{Z'}^2 \Gamma_{Z'}^2} \right) \\ &\times \left\{ 2C_F([12] + [34]) \right\} \\ &+ \frac{g_s^4 g'^2}{N_c} 2\text{Re} \left(\frac{(u^2 + t^2)\{vv'\} + (u^2 - t^2)\{aa'\}}{s[s - M_{Z'}^2 + iM_{Z'}\Gamma_{Z'}]} \right) \\ &\times \left\{ 2C_F([13] + [24] - [14] - [23]) \right\} \end{aligned} \quad (\text{A4})$$

$$q(p_1) + q'(p_2) \rightarrow q(p_3) + q'(p_4) + g(k)$$

$$\begin{aligned}
\overline{\Sigma}|\mathcal{M}|^2 &= \frac{g_s^6 C_F}{N_c} \left(\frac{s^2 + u^2}{t^2} \right) \left\{ 2C_F([14] + [23]) + \frac{1}{N_c}[12; 34] \right\} \\
&+ 2g_s^2 g'^4 \left(\frac{(s^2 + u^2)\{(v^2 + a^2)(v'^2 + a'^2)\} + (s^2 - u^2)\{4vav'a'\}}{(t - M_{Z'}^2)^2 + M_{Z'}^2 \Gamma_{Z'}^2} \right) \\
&\times \left\{ 2C_F([13] + [24]) \right\} \\
&+ \frac{g_s^4 g'^2}{N_c} 2\text{Re} \left(\frac{(s^2 + u^2)\{vv'\} + (s^2 - u^2)\{aa'\}}{t[t - M_{Z'}^2 + iM_{Z'}\Gamma_{Z'}]} \right) \\
&\times \left\{ 2C_F([14] + [23] - [12] - [34]) \right\}
\end{aligned} \tag{A5}$$

$$q(p_1) + q(p_2) \rightarrow q(p_3) + q(p_4) + g(k)$$

$$\begin{aligned}
\overline{\Sigma}|\mathcal{M}|^2 &= \frac{g_s^6 C_F}{N_c} \left(\frac{s^2 + u^2}{t^2} - \frac{1}{N_c} \frac{s^2}{tu} \right) \left\{ 2C_F([14] + [23]) + \frac{1}{N_c}[12; 34] \right\} \\
&+ \frac{g_s^6 C_F}{N_c} \left(\frac{s^2 + t^2}{u^2} - \frac{1}{N_c} \frac{s^2}{tu} \right) \left\{ 2C_F([13] + [24]) + \frac{1}{N_c}[12; 34] \right\} \\
&- \frac{g_s^6 C_F}{N_c} \frac{s^2}{tu} \left(1 - \frac{1}{N_c^2} \right) \left\{ [12; 34] \right\} \\
&+ \frac{g_s^4 g'^2}{N_c} 2\text{Re} \left(\frac{(s^2 + u^2)\{v^2\} + (s^2 - u^2)\{a^2\}}{t[t - M_{Z'}^2 + iM_{Z'}\Gamma_{Z'}]} \right) \\
&\times \left\{ 2C_F([14] + [23] - [12] - [34]) \right\} \\
&+ \frac{g_s^4 g'^2}{N_c} 2\text{Re} \left(\frac{(s^2 + t^2)\{v^2\} + (s^2 - t^2)\{a^2\}}{u[u - M_{Z'}^2 + iM_{Z'}\Gamma_{Z'}]} \right) \\
&\times \left\{ 2C_F([13] + [24] - [12] - [34]) \right\} \\
&+ g_s^4 g'^2 \frac{C_F}{N_c} 2\text{Re} \left(\frac{2s^2\{v^2 + a^2\}}{t[u - M_{Z'}^2 + iM_{Z'}\Gamma_{Z'}]} \right) \\
&\times \left\{ 2C_F([23] + [14]) + \frac{1}{N_c}([12] + [34] - [13] - [24]) \right\} \\
&+ g_s^4 g'^2 \frac{C_F}{N_c} 2\text{Re} \left(\frac{2s^2\{v^2 + a^2\}}{u[t - M_{Z'}^2 + iM_{Z'}\Gamma_{Z'}]} \right) \\
&\times \left\{ 2C_F([13] + [24]) + \frac{1}{N_c}([12] + [34] - [23] - [14]) \right\} \\
&+ 2g_s^2 g'^4 \left(\frac{(s^2 + u^2)\{(v^2 + a^2)^2\} + (s^2 - u^2)\{4v^2 a^2\}}{(t - M_{Z'}^2)^2 + M_{Z'}^2 \Gamma_{Z'}^2} \right) \\
&\times \left\{ 2C_F([13] + [24]) \right\}
\end{aligned}$$

$$\begin{aligned}
& + 2g_s^2 g'^4 \left(\frac{(s^2 + t^2)\{(v^2 + a^2)^2\} + (s^2 - t^2)\{4v^2 a^2\}}{(u - M_{Z'}^2)^2 + M_{Z'}^2 \Gamma_{Z'}^2} \right) \\
& \times \left\{ 2C_F([23] + [14]) \right\} \\
& + \frac{g_s^2 g'^4}{N_c} 2\text{Re} \left(\frac{s^2 \{(v + a)^4 + (v - a)^4\}}{[u - M_{Z'}^2 + iM_{Z'} \Gamma_{Z'}][t - M_{Z'}^2 - iM_{Z'} \Gamma_{Z'}]} \right) \\
& \times \left\{ 2C_F([13] + [14] + [23] + [24] - [12] - [34]) \right\}
\end{aligned} \tag{A6}$$

$$q(p_1) + \bar{q}(p_2) \rightarrow g(p_3) + g(p_4) + g(k)$$

$$\begin{aligned}
\overline{\sum} |\mathcal{M}|^2 &= g_s^6 C_F (t^2 + u^2) \left[\left(1 - \frac{1}{N_c^2} \right) \frac{1}{tu} - \frac{2}{s^2} \right] \left\{ 2C_F[12] + 2N_c[34] \right\} \\
& - \frac{g_s^6 N_c}{4} (t^2 + u^2) \left[\left(1 - \frac{2}{N_c^2} \right) \frac{1}{tu} - \frac{2}{s^2} \right] \left\{ 2C_F[12; 34] \right\} \\
& + \frac{g_s^6 N_c}{4} (t^2 - u^2) \left[\frac{1}{tu} - \frac{2}{s^2} \right] \left\{ 2C_F([14] + [23] - [13] - [24]) \right\}
\end{aligned} \tag{A7}$$

$$q(p_1) + g(p_2) \rightarrow q(p_3) + g(p_4) + g(k)$$

$$\begin{aligned}
\overline{\sum} |\mathcal{M}|^2 &= \frac{g_s^6}{2} (s^2 + u^2) \left[\left(1 - \frac{1}{N_c^2} \right) \frac{1}{-su} + \frac{2}{t^2} \right] \left\{ 2C_F[13] + 2N_c[24] \right\} \\
& - \frac{g_s^6 N_c^2}{4(N_c^2 - 1)} (s^2 + u^2) \left[\left(1 - \frac{2}{N_c^2} \right) \frac{1}{-su} + \frac{2}{t^2} \right] \left\{ 2C_F[13; 24] \right\} \\
& + \frac{g_s^6 N_c^2}{4(N_c^2 - 1)} (s^2 - u^2) \left[\frac{1}{-su} + \frac{2}{t^2} \right] \left\{ 2C_F([14] + [23] - [12] - [34]) \right\}
\end{aligned} \tag{A8}$$

$$g(p_1) + g(p_2) \rightarrow g(p_3) + g(p_4) + g(k)$$

$$\begin{aligned}
\overline{\sum} |\mathcal{M}|^2 &= \frac{4g_s^6 N_c^2}{N_c^2 - 1} \left[3 - \frac{ut}{s^2} - \frac{us}{t^2} - \frac{st}{u^2} \right] \left\{ \frac{2}{3} N_c([12] + [34] + [13] + [14] + [23] + [24]) \right\} \\
& + \frac{2g_s^6 N_c^2}{3(N_c^2 - 1)} \left[3 + \frac{st}{u^2} + \frac{us}{t^2} - 2\frac{ut}{s^2} - 3\frac{s^2}{ut} \right] \left\{ N_c([12] + [34]) \right\} \\
& + \frac{2g_s^6 N_c^2}{3(N_c^2 - 1)} \left[3 + \frac{st}{u^2} + \frac{ut}{s^2} - 2\frac{us}{t^2} - 3\frac{t^2}{us} \right] \left\{ N_c([13] + [24]) \right\} \\
& + \frac{2g_s^6 N_c^2}{3(N_c^2 - 1)} \left[3 + \frac{ut}{s^2} + \frac{us}{t^2} - 2\frac{st}{u^2} - 3\frac{u^2}{st} \right] \left\{ N_c([14] + [23]) \right\}
\end{aligned} \tag{A9}$$

Several comments are in order concerning the colour-suppressed interference contributions which appear in the above results. We note first that they are not singular when the soft gluon is collinear with either the initial- or final-state partons. Secondly, only two of them are actually independent. To see this we introduce the following notation for the “dipole” combinations:

$$\begin{aligned} I_a &= [13] + [24] - [14] - [23] , \\ I_b &= [14] + [23] - [12] - [34] , \\ I_c &= [13] + [24] - [12] - [34] . \end{aligned} \tag{A10}$$

Then it follows that (see Ref. [8])

$$\begin{aligned} I_a + I_b &= I_c , \\ I_a + I_c &= [13; 24] , \\ I_b - I_a &= [14; 23] , \\ [13; 24] + [14; 23] &= -[12; 34] . \end{aligned} \tag{A11}$$

Note that interchanging $p_3 \leftrightarrow p_4$ gives

$$\begin{aligned} I_a &\rightarrow -I_a , \\ I_b &\rightarrow I_c , \\ [12; 34] &\rightarrow [12; 34] , \\ [13; 24] &\rightarrow [14; 23] . \end{aligned} \tag{A12}$$

References

- [1] CDF Collaboration: F. Abe et al., Phys. Rev. Lett. **77** (1996) 438.
- [2] DØ Collaboration: G.C. Blazey, presented at the XXXI Rencontres de Moriond, QCD and High Energy Hadronic Interactions, Les Arcs, France, March 1996, Fermilab-Conf-96-132-E (1996).
- [3] G. Altarelli, N. Di Bartolomeo, F. Feruglio, R. Gatto and M. Mangano, CERN preprint CERN-TH/96-20 (1996).
P. Chiappetta, J. Layssac, F.M. Renard and C. Verzegnassi, Marseille preprint CPT-96-P-3304 (1996).
- [4] V. Barger, M.S. Berger and R.J.N. Phillips, Madison preprint MADPH-95-920 (1995).
J. Ellis and D.A. Ross, preprint CERN-TH/96-108 (1996).
P. Kraus and F. Wilczek, Caltech preprint CALT-68-2032 (1996).
- [5] CTEQ Collaboration: J. Huston et al., Michigan State preprint MSU-HEP-50812 (1995); H.L. Lai and W.-K. Tung, Michigan State preprint MSU-HEP-60508 (1996).

- [6] E.W.N. Glover, A.D. Martin, R.G. Roberts and W.J. Stirling, Durham preprint DTP/96/22 (1996), to be published in Phys. Lett.
- [7] E.J. Eichten, K. Lane and M.E. Peskin, Phys. Rev. Lett. **50** (1983) 811.
- [8] Yu.L. Dokshitzer, V.A. Khoze and S.I. Troyan, in Proc. 6th Int. Conf. on Physics in Collision, ed. M. Derrick (World Scientific, Singapore, 1987), p.417.
Yu.L. Dokshitzer, V.A. Khoze and S.I. Troyan, Sov. J. Nucl. Phys. **46** (1987) 712.
- [9] Yu.L. Dokshitzer, V.A. Khoze, A.H. Mueller and S.I. Troyan, Rev. Mod. Phys. **60** (1988) 373.
Yu.L. Dokshitzer, V.A. Khoze and S.I. Troyan in: Advanced Series on Directions in High Energy Physics, Perturbative Quantum Chromodynamics, ed. A.H. Mueller (World Scientific, Singapore), v. 5 (1989) 241.
- [10] Yu.L. Dokshitzer, V.A. Khoze, A.H. Mueller and S.I. Troyan, “Basics of Perturbative QCD”, ed. J. Tran Thanh Van, Editions Frontières, Gif-sur-Yvette, 1991.
- [11] B. Andersson, B. Gustafson, G. Ingelman and T. Sjöstrand, Phys. Rep. **97** (1983) 31.
- [12] B. Andersson, G. Gustafson and T. Sjöstrand, Phys. Lett. **B94** (1980) 211.
- [13] Ya.I. Azimov, Yu.L. Dokshitzer, V.A. Khoze and S.I. Troyan, Phys. Lett. **B165** (1985) 147; Sov. J. Nucl. Phys. **43** (1986) 95.
- [14] T. Hebbeker, Phys. Rep. **217** (1992) 69.
- [15] M. Schmelling, Physica Scripta **51** (1995) 683.
- [16] CDF Collaboration: F. Abe et al., Phys. Rev. **D50** (1994) 5562. D0 Collaboration: S. Abachi et al., FERMILAB preprint, FERMILAB Conf-95/182-E.
N. Varelas, preprint FERMILAB, Conf-95/181-E, D0 and CDF; presented at the XXXI Rencontres de Moriond, Les Arcs, Savoie, France, March 23-30, 1996.
- [17] G. Marchesini and B.R. Webber, Nucl. Phys. **B310** (1988) 461.
G. Marchesini, B.R. Webber, G. Abbiendi, I.G. Knowles, M.H. Seymour and L. Stanco, Comp. Phys. Commun. **67** (1992) 465.
- [18] T. Sjöstrand, Comp. Phys. Commun. **39** (1986) 347.
T. Sjöstrand and M. Bengtsson, Comp. Phys. Commun. **43** (1987) 367.
T. Sjöstrand, CERN preprint CERN-TH 6488/92 (1992).
- [19] L. Lönnblad, Comp. Phys. Commun. **71** (1992) 15.
- [20] W.T. Giele, E.W.N. Glover and D.A. Kosower, Nucl. Phys. **B403** (1993) 633.
- [21] Yu.L. Dokshitzer, V.A. Khoze and S.I. Troyan, Sov. J. Nucl. Phys. **50** (1989) 505; see also Ref. [8].

- [22] V.A. Khoze, in Proc. Int. Symp. on Lepton and Photon Interactions, Stanford, 1989, ed. M. Riordan (World Scientific, Singapore, 1990), p.387.
- [23] Yu.L. Dokshitzer, V.A. Khoze and T. Sjöstrand, Phys. Lett. **B274** (1992) 116.
- [24] G. Marchesini and B.R. Webber, Nucl. Phys. **B330** (1990) 261.
- [25] D. Zeppenfeld, Madison preprint MADPH-95-933 (1996).
- [26] R.K. Ellis, G. Marchesini and B.R. Webber, Nucl. Phys. **B286** (1987) 643; Erratum Nucl. Phys. **B294** (1987) 1180.
R.K. Ellis, presented at “Les Rencontres de Physique de la Vallée d’Aoste”, La Thuile, Italy, March 1987, preprint FERMILAB-Conf-87/108-T (1987).
- [27] V.A. Khoze, L.H. Orr and W.J. Stirling, Nucl. Phys. **B378** (1992) 413.
Yu.L. Dokshitzer, V.A. Khoze, L.H. Orr and W.J. Stirling, Nucl. Phys. **B403** (1993) 65.
V.A. Khoze, J. Ohnemus and W.J. Stirling, Phys. Rev. **D79** (1994) 1237.
- [28] G. Altarelli *et al.*, Ref. [3].
- [29] B. Andersson, H.-U. Bengtsson, G. Gustafson and B. Nilsson-Almqvist, Lund preprint LU TP 84-11 (1984).
- [30] T. Sjöstrand and V.A. Khoze, Z. Phys. **C62** (1994) 281.
- [31] F.A. Berends, R. Kleiss, P. de Causmaecker, R. Gastmans and T.T. Wu, Phys. Lett. **B103** (1981) 102.
- [32] A.D. Martin, R.G. Roberts and W.J. Stirling, Durham preprint DTP/96/44 (1996), to be published in Phys. Lett.
- [33] E.J. Eichten, I. Hinchliffe, K. Lane and C. Quigg, Rev. Mod. Phys. **56** (1984) 579; Phys. Rev. **D34** (1986) 1547.
K. Lane, Boston University preprint BUHEP-96-8 (1996).